

# Chapter 1: Introduction and Literature Review

---

The International Energy Agency (IEA) reports that the world's energy consumption has almost doubled between 1973 and 2013, from  $5.42 \times 10^7$  kWh to  $1.08 \times 10^8$  kWh [1], and as the demand for energy continues to increase it is estimated that by 2050 world energy supplies will have to double again to reach demand [2]. With climate change becoming an increasing issue, research continues to develop more efficient, safe and environmentally friendly methods to produce energy. It has been suggested by the IEA that nuclear and renewable energy are likely sources of clean energy in the future, and research is currently ongoing to allow this to happen [3].

The Generation IV International Forum (GIF), an international cooperative which aims to research and develop the next generation of nuclear reactors, have identified six different systems which they believe can achieve their four goal areas [4]:

- sustainability
- safety and reliability
- proliferation resistance and physical protection
- economic competitiveness

The six reactor systems that were selected by the GIF in 2002 were:

- gas cooled fast reactor (GFR)
- lead cooled fast reactor (LFR)
- molten salt reactor (MSR)
- sodium cooled fast reactor (SFR)
- supercritical water-cooled reactor (SCWR)
- very high temperature reactor (VHTR)

With continuing research, it is envisaged that each of these reactors will be able to produce energy while also attaining the original four goals [4].

The work in this thesis will focus on molten salt reactors, which produce energy in a unique way compared to the current operational fleet. One of the main research drivers is the corrosion resistance of the material of containment, as the fuel salt and coolant are highly corrosive in the presence of any impurities [5].

## 1.1 Molten Salt Reactors

Molten salt reactors are different to conventional water based reactors as they utilise a liquid fuel, mixed in with the heat transfer medium. The molten salt, made up of a mixture of lithium and beryllium fluoride salts (FLiBe), together with fissile and fertile material such as ThF<sub>4</sub> (thorium tetrafluoride) and UF<sub>4</sub> (uranium tetrafluoride) flows through a reactor core. This can be graphite moderated or not depending on if an epithermal or thermal neutron system is required [6, 7]. The salt subsequently flows through to a heat exchanger where heat is transferred to a non-radioactive salt, usually NaBF<sub>4</sub>-NaF (sodium tetrafluoroborate-sodium fluoride) [8]. This heated salt then flows through a secondary circuit where water is converted to steam, driving a steam turbine, generating electricity in the conventional way. This type of reactor tends to operate between 400 and 900°C [6].

A schematic of a molten salt reactor is given in Figure 1.1.

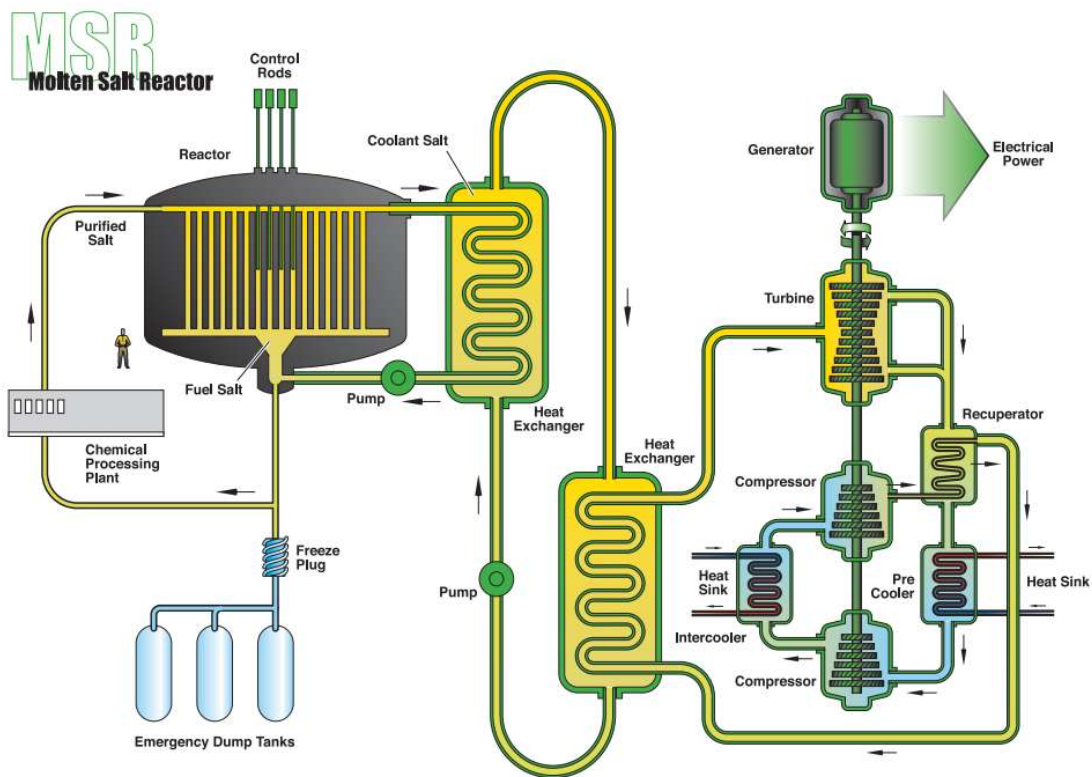


Figure 1.1: Schematic of a molten salt reactor using a graphite moderated reactor core [4].

As previously mentioned, the aim of the GenIV reactors is to produce energy while also attaining the four goals set out by the GIF. The first aim was for the system to be sustainable, i.e. primarily a closed fuel cycle, which in turn minimises waste going to a repository. As most actinides and fission products readily form fluorides it is possible to fully recycle actinides and with it being a liquid fuel, refuelling,

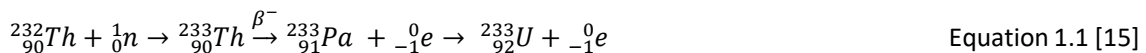
processing and fission product removal can all be done while the reactor is operating. The liquid fuel also allows for variation in compositions to be used, and complex fuel fabrication is not required as it is with a solid reactor [4, 9, 10]. It is also possible for the MSR to produce electricity from hydrogen due to the high outlet temperatures that can be achieved by the reactor [4].

The GIF have classed the MSR as top ranked for sustainability as a closed fuel cycle can be achieved along with excellent waste burndown [4].

It has been noted that there is uncertainty with economic predictions for all six GenIV reactor systems as none have been deployed, therefore production and capital costs are estimations [4], but studies by Moir (2002) and by MacPherson (1985) [11, 12] have suggested that the cost of a MSR would be competitive with coal, PWR (pressurised water reactors) and LWR (light water reactors).

Evaluating the proliferation resistance of the MSR is problematic due to the lack of regulations for liquid fuelled reactors, as all civilian nuclear reactors currently utilise solid fuel. It is believed that this system is proliferation resistant, as obtaining weapon grade nuclear material will be difficult due to the liquid nature of the fuel. Uranium is substantially diluted in the salt, and to obtain the amount required for a weapon would require a chemical plant capable of handling tonnes of uranium [13]. As chemical reprocessing units have yet to be fully designed, it is difficult to quantify how proliferation resistant the MSR will be.

Despite there being a lack of knowledge in the proliferation resistance of the MSR systems, work has been done to determine the proliferation resistance of the thorium fuel cycle. Kang and Von Hippel [14] investigated the production of weapons grade uranium-233 in the thorium fuel cycle. Equation 1.1 shows the production of uranium-233 from thorium-232.



One major concern when handling uranium-233 is that it often appears concurrently with uranium-232 and it is difficult to separate. Uranium-232 decays to thallium-208 which emits a strong gamma ray during decay, which requires significant shielding. Conversely, the plutonium decay chain can produce americium-241, which emits gamma rays with a significantly lower energy (0.1 MeV) [14].

The major safety feature of the MSR is the low vapour pressure of the fuel salt, which reduces stress on the structure, coupled with a relative high boiling point, this allows the system to run without pressurisation and decreases the stress on the reactor system. The system also has a strong negative temperature and void coefficient, meaning that as the temperature increases within the core, the efficiency of the core decreases, bringing the reaction under control [16, 17].

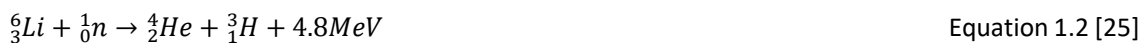
There are other inherently safe properties of the system such as: passive cooling, low inventory of volatile fission products and fail-safe drainage into passively cooled dump tanks, which can be seen in Figure 1.1. If there is a power outage the actively cooled freeze plug melts and the molten salt is dumped into the tanks and solidifies, trapping dangerous fission products. This allows the reactor to be classed as passively cooled [18].

In addition to this, any off-gases produced from the nuclear reaction, such as xenon and krypton, are removed directly by a system designed to trap the gases and make them easier and safer to handle [19]. Many fission products form stable fluoride compounds or are highly volatile so they can be continually removed from the system [20].

In addition to the four goals set out by the GIF, MSR's exhibit other useful properties, such as a high heat capacity, which increases thermodynamic efficiency resulting in more energy being transferred. [20]. The thermodynamic properties of an MSR allows for it to be coupled to a hydrogen production plant, and there is also the potential for it to be used as a heat transfer medium in the very high temperature reactor (VHTR) due to its high heat capacity. Molten salts are also transparent, which aids in inspection, and are not damaged by radiation [21, 22].

Investigations conducted by the GIF have identified technology gaps in the six systems, and the latest roadmap published in January 2014 addresses some of these issues [23]. The key issue, which is the focus of this work, is compatibility of the molten salt with structural materials at high temperatures within the reactor. Other issues have also been identified such as the molten salt chemistry, which will themselves require extensive research before the system can be approved [23].

Further issues with this system include tritium formation and control, arising from the use of lithium within the core, which is discussed in further detail in Section 1.2. Tritium is formed via neutron absorption and the reaction is given in Equation 1.2. Due to its small molecular size it is possible for tritium to diffuse through the heat exchanger walls, making the non-radioactive salt radioactive and jeopardising the secondary circuit [24].



### *1.1.1: History of Molten Salt Reactors*

Despite the GIF identifying the molten salt reactor as a new design, Oak Ridge National Laboratory have previously developed, built and operated two molten salt reactors in the 1950's and 60's.

The first reactor was the Aircraft Reactor Experiment (ARE), designed and operated by ORNL, and was part of the Aircraft Nuclear Propulsion (ANP) programme, which ran between 1946-1951. The aim was to produce a nuclear powered aircraft [26, 27].

Molten salts were proposed as they gave a high power density, along with high operating temperatures, which as previously mentioned enhances efficiency. The increased safety of the negative void and temperature coefficient, helping to prevent temperature excursions was another. Thus they gave the aircraft a level of self-stabilisation, which was difficult to achieve with solid fuel [26].

The aim of ARE was to develop a low power experimental reactor to address uncertainties raised in previous research. A mixture of NaF/ZrF<sub>4</sub>/UF<sub>4</sub> (sodium fluoride, zirconium tetrafluoride and uranium tetrafluoride) (54/41/6 wt. %) was used with the uranium enriched to 93.4% <sup>235</sup>U. By comparison, in modern LWRs enrichment is usually 3-5 wt. %. Beryllium oxide moderators were required, as molten fluorides containing uranium did not appear to have the ability to moderate the energy of the neutrons. Inconel 600 was chosen as the material of construction. The reactor ran in 1954 for nine days and no problems were encountered, with temperature ranging between 663-860°C with a power output of 2.5 MW [26, 28, 29]. However, numerous other issues were identified with this programme, such as the large reactor needed to get the craft airborne, and the shielding requirements to keep the flight crew safe [30].

Although the ARE itself was cancelled, further work was undertaken by ORNL to develop a molten salt breeder reactor for civilian power generation. Initially the Molten Salt Reactor Experiment (MSRE) was built with no breeding capability, designed to test new salts and structural materials. It operated for six months in 1965 with no reported issues. After a full investigation into the ARE numerous changes were made to the MSRE, including the utilisation of a graphite moderator along with a different fuel salt, <sup>7</sup>LiF-BeF<sub>2</sub>-ZrF<sub>4</sub>-UF<sub>4</sub> (lithium fluoride, beryllium fluoride, zirconium tetrafluoride and uranium tetrafluoride) (65-29.15-0.8 wt. %) and FLiBe (LiF-BeF<sub>2</sub>) was employed as a coolant. Lithium-7 was utilised due to its enhanced neutronic properties, whilst BeF<sub>2</sub> both lowered the melting point of the salt, and provided a neutron source increasing neutron efficiency. A new structural material Hastelloy N was developed; this new alloy was optimised to reduce the corrosion observed in Inconel 600 during the ARE and was also code qualified for use in molten salts up to 750°C. The MSRE ran with a

temperature range of 635-662°C with a maximum power output of 8 MWt [8, 20, 31]. A design was proposed by ORNL for a breeder reactor which used  $\text{LiF-BeF}_2\text{-ThF}_4\text{-UF}_4$  as a fuel salt with  $\text{NaF-NaBF}_4$  as a coolant, but before the reactor could be developed further the programme was cancelled and research concentrated on sodium fast reactors [17, 32].

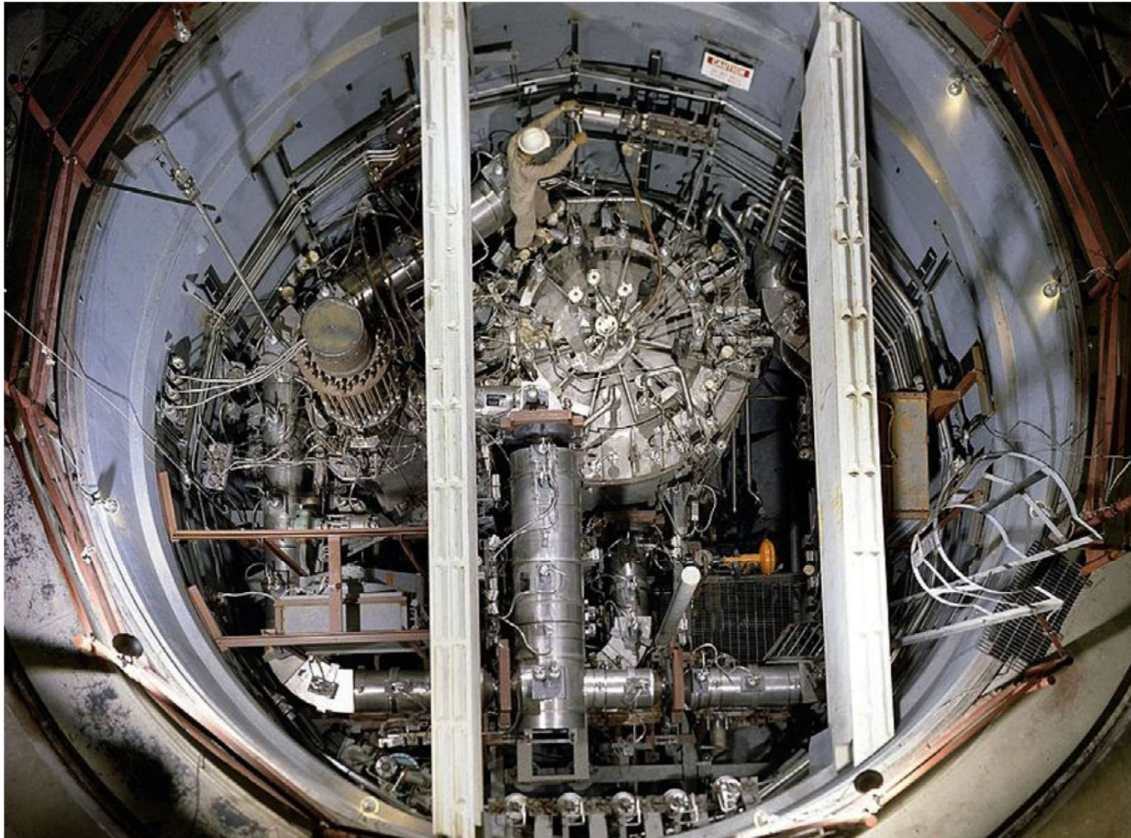


Figure 1.2: MSRE test reactor [17].

## 1.2: Selection of Molten Salt

Molten salts are by their very nature non-aqueous solvents, and can be utilised as both a fuel medium and coolant. Molten salts have a high boiling temperature, high heat capacity, low vapour pressure and high temperatures can be employed due to the increased thermodynamic efficiency [22]. The choice of salt is important as different salts interact with the fuel and also the structural material in different ways. The salt must have favourable physical, chemical and neutronic properties [31, 33].

Chemical and physical considerations that need to be addressed are corrosion of the structural material, high heat capacity, low vapour pressure and the melting temperature. It is possible to form a eutectic, a mixture of two or more salts with a significantly lower melting temperature compared to single salts. A binary eutectic can lower the melting temperature of the salt by as much as 500°C, but

the addition of a further salt to make a ternary eutectic may only lower the melting temperature by 50°C [34]. Therefore the third salt needs to show desirable properties within the system for it to be added. It is possible for the salt to exhibit some of the properties of water, such as high heat transfer at high temperatures, but without the high pressures required. Further requirements include high solubility of the fuel within the salt, low viscosity and high chemical stability of the salt [17, 20, 31].

As previously mentioned, two MSR's have been successfully run by ORNL, each with a different fuel salt. The salt choice for the aircraft reactor experiment (ARE) was the only fluid fuel that was available to ORNL at the time and consisted of NaF-ZrF<sub>4</sub>-UF<sub>4</sub> [27]. It was found in the ARE that nearly all of the vapour over the salt was ZrF<sub>4</sub>, which was being deposited as solid ZrF<sub>4</sub>. This was found in the piping and therefore some ZrF<sub>4</sub> was not returning to the reactor core [34]. In the MSRE a much lower vapour pressure was employed; this was due to the salt used, a mixture of UF<sub>4</sub>-<sup>7</sup>LiF-BeF<sub>2</sub>-ZrF<sub>4</sub>. The cations in the MSRE were chosen due to their chemical stability, which was intended to reduce corrosion in the system. ZrF<sub>4</sub> was added to prevent the precipitation of UO<sub>2</sub>. The ratio of LiF to BeF<sub>2</sub> within the MSRE fuel was chosen to optimise the requirements for low viscosity and liquidus temperature. The vapour above the salt was LiF-BeF<sub>2</sub>; this melted at a lower temperature and therefore condensed and was circulated back to the reactor [22, 31].

### *1.2.1: Salt Choice for this Work*

When research into fluid fuel reactors was in its infancy numerous different salts were investigated, for example, carbonates, nitrates/nitrites, fluorides and chlorides. Oxygenated anions such as nitrates and nitrites (NO<sub>3</sub><sup>-</sup> and NO<sub>2</sub><sup>-</sup>) did not exhibit good thermal stability, as they were found to decompose at around 600°C, and carbonates (CO<sub>3</sub><sup>2-</sup>) could not dissolve a high enough concentration of thorium compounds [35, 36]. It was determined that halides displayed the most favourable properties with fluorides being preferred over chlorides due to the high neutron cross section of chlorine-35, which makes up approximately 75% of naturally occurring chlorine [37]; this can be resolved by separating <sup>35</sup>Cl from <sup>37</sup>Cl, but this is difficult and costly. In addition to the high neutron cross section, a long lived isotope chlorine-36, with a half-life of approximately 301,000 years, is produced via chlorine-35 neutron capture, and reduces the efficiency of the reactor. Chlorides are also soluble in water and therefore it is possible that they will be released from a repository. Fluorides are less of an issue as they can form insoluble wastefoms and are inert to some structural materials [20, 33, 36].

Work done by Oak Ridge National Laboratory highlighted numerous advantages for the utilisation of fluoride salts, these include: low capture cross section (0.009 barns), high solubility of uranium and thorium, along with its low vapour pressure, which could not be achieved in an aqueous homogenous reactor [31, 33]. Work has also been undertaken investigating the radiolysis of fluoride salts, and it

was found that none was observed in either fluoride or fluoroborate salts [38, 39]. Further studies have suggested that molten fluorides are radiolytically stable and therefore any effect on corrosion due to radiolysis is expected to be insignificant. Salts used in the ARE and MSRE showed no detectable issues and both salts were resistant to reactor radiation, uranium fission and accumulation of fission products. Generally, radiation will dissociate fluorides and the recombination effects are kinetically favourable in molten salt [20, 31].

Other advantages of fluorides are their thermodynamic stability, inertness to some structural materials, potential for good heat transfer capabilities, high heat capacities, and often low vapour pressure [6, 31]. Finally, fluorine is monoisotopic, meaning that, unlike chlorine, it has only one naturally stable isotope, making it easier to separate [17].

Although fluorides are the main area of research for fluid reactor fuel, some disadvantages have been noted. Fluoride salts are not good moderators and therefore materials such as beryllium oxide (BeO) in the ARE and graphite in the MSRE were employed as moderators. The high melting temperature of the salts is also considered a disadvantage as an external heating system is required to prevent freezing in the pipes [31, 33]. However, this disadvantage can also be viewed as an advantage in the case of any salt spillages as the salt will freeze and prevent any release of fission products [16, 31, 40].

Further problems were identified that include the corrosion resistance of the structural material in contact with the salt and the high concentration of fuel required compared to an aqueous system.

Chlorides were considered as a secondary coolant, but chlorides are easily reduced, which can lead to an increase in the corrosion of structural materials [35]. Coolants must possess the ability to melt at useful temperatures, have low volatility, and show chemical stability [41].

This work utilises chlorides as it is not currently feasible to conduct this experimental work with fluorides in the laboratory. It is stated by Ignatiev and Surenkov [42] that chlorides have a more corrosive nature than fluorides, but within a scoping test this can be seen as advantageous [42].

The cations used in the fluoride system were also extensively studied, and some of that work will be discussed here. The composition of the fuel salt is important and can dramatically change the properties of the salt, such as toxicity and neutron activation. Some salts can produce tritium whereas others can produce gamma emitting radionuclides, therefore the choice of the salt will influence the shielding and other controls that will be required. Consequently, the salt needs to be specifically designed for its purpose; electropositive elements that show favourable dynamics along with a low neutron capture cross section include lithium-7 ( ${}^7\text{Li}$ ), beryllium (Be), sodium (Na), rubidium (Rb) and zirconium (Zr). Fluids that can be utilised in a liquid fuelled/cooled reactor are alkali fluorides, mixtures

of alkali fluorides and beryllium fluoride, and mixtures of alkali fluorides with zirconium fluoride, as they have shown low melting temperatures, material compatibility, and also acceptable neutronics [20, 41].

Lithium fluoride makes up part of the most viable fluoride salt mixtures (FLiBe), primarily due to it being a good moderator, lowering the viscosity of the beryllium fluoride constituent, and appearing to reduce corrosion of the structural material. The use of beryllium introduces new risks due to its high toxicity, and so this should only be used if no alternative can be found [31]. The utilisation of lithium does have problems as tritium is produced via lithium-6 within the system, as shown in Equation 1.2. Therefore, the lithium needs to be purified so only lithium-7 remains, this will give enhanced neutronics but will be costly [19].

Different fluoride salts have been investigated; alkali fluorides, alkali earth fluorides and zirconium fluorides are non-toxic, and alkali fluorides combined with zirconium fluoride giving a low tritium yield. The addition of  $ZrF_4$  tends to lower the vapour pressure and prevents the precipitation of  $UO_2$  [20]. Although beryllium fluoride is named as one of the possible constituents of a fluid fuel, it does have one disadvantage: if too much is added it can form a highly viscous liquid, which will need to be accounted for when designing any pump systems [41]. It was also found that rubidium and sodium atoms more readily donate fluoride atoms to beryllium compared to lithium-7, therefore it is possible to substitute salts to reduce this phenomenon. Potassium containing salts are usually avoided due to their high neutron cross section, but FLiNaK (LiF-NaF-KF) is often used as a reference salt [31].

Current research is focused on the use of the fuel salt FLiBe, a eutectic mixture of LiF- $BeF_2$  (66-33 mol. %) [43], which is stable, has a low corrosion rate and also when lithium-7 is incorporated has good neutronics for use as a fluid fuel. FLiNaK, which is a eutectic mixture of LiF-NaF-KF (46.5-11.5-42 mol. %) [31], is often used for research purposes as toxic  $BeF_2$  is omitted, but potassium has a higher neutron cross section and therefore is unlikely to be used in a fuel [31, 44, 45]. This work will use lithium, potassium and sodium due to the high levels of toxicity associated with beryllium.

### 1.3: Materials for MSR's

Historically nickel superalloys have been used as the material of construction for molten salt reactors due to their enhanced corrosion resistance during testing [26].

Work done by Richardson et al. [46] for ORNL examined the surface corrosion of a range of alloys (300 and 400 stainless steels, Inconels, Hastelloys, vanadium and molybdenum) using static and dynamic testing. It was found that the depth of attack was less for the tested stainless steels compared to

Inconel, but as the paper focuses primarily on the corrosion of nickel alloys and in particular Inconel it is difficult to determine why stainless steel was not suggested as a material of construction [46].

Although stainless steel has not been used within a molten salt reactor, work has been conducted relating to stainless steel corrosion in molten salts for processes such as thermal energy storage, solar cells and pyrochemical reprocessing [47-49]. It is envisaged that this research will be useful in implementing further research into the utilisation of stainless steel within the molten salt reactor. Work by Sarvghad et al. [47] investigated stainless steel 316 in three different eutectic salts at 700°C, and uniform corrosion was observed, with the most aggressive salt being Na<sub>2</sub>CO<sub>3</sub>. This result is promising as although carbonates are unlikely to be used in a reactor due to the problems stated in Section 1.2, it proves that stainless steel can be used within a molten salt environment. It is also possible that a new stainless steel could be developed to give favourable corrosion properties.

### *1.3.1: Nickel Superalloys*

Only two molten salt reactors have been built and operated; the MSRE and the ARE, both used different nickel-based superalloys as structural materials. The first reactor used Inconel 600 and the second reactor used a more refined version called Hastelloy N. The compositions of these two materials are given in Table A.1 in the Appendix.

The principal difference between these two alloys is in the chromium and molybdenum content. Molybdenum is added to strengthen the alloy and is controlled such that the solid solution alloy would be stable across a wider range of temperatures. However, it was found that alloys with a higher molybdenum content exhibited embrittlement between 650-815°C. There is also a significant decrease in the chromium content of Hastelloy N. This is due to an oxidation rate change when the chromium content is approximately 6 wt. %, changing the oxide from NiMoO<sub>4</sub> to Cr<sub>2</sub>O<sub>3</sub> [31, 36]. Numerous investigations have identified that corrosion of nickel based superalloys predominantly arises from dealloying of chromium, as a consequence the chromium content was kept to a minimum [46, 50, 51]. Chromium dealloying is shown in Figure 1.3, where chromium depletion can be seen after Hastelloy N has been immersed in FLiNaK [52].

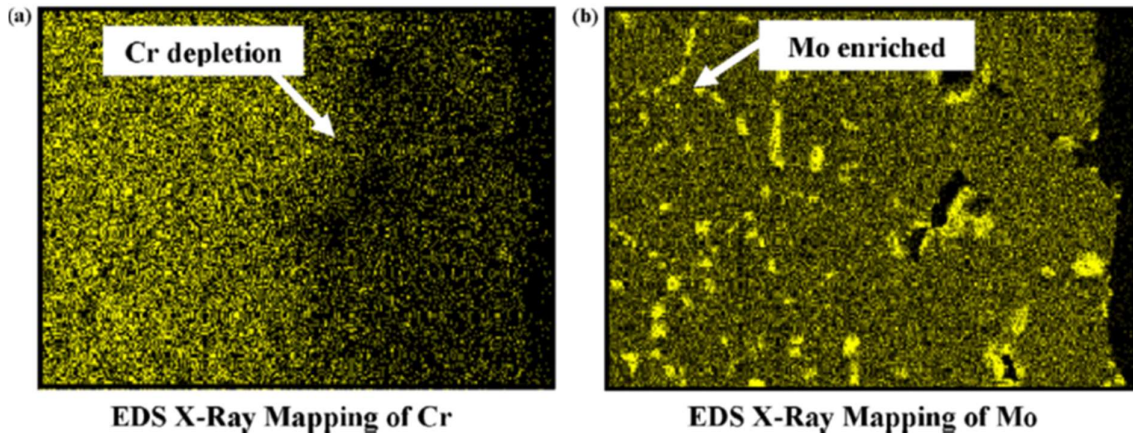


Figure 1.3: Cross sectional EDS of Hastelloy N that has been immersed in FLiNaK at 850°C for 500 hours, from Olson et al. [52].

Further investigation during the operation of the MSRE showed that Hastelloy N suffered significant embrittlement arising from irradiation at high temperatures, with observed intergranular cracking attributed to tellurium although the quantity present was not reported. It was believed that these problems could be directly credited to the material composition [53].

It was also noted by Richardson et al. [46] that the major form of attack when Inconels were submerged in molten fluorides was void formation, scattered uniformly over the entire surface or limited to grain boundaries. It has been suggested that when chromium, the alloying addition most likely to be attacked diffuses into the salt, migration occurs and it is possible that these vacancies coalesce to form voids. [36, 46].

### 1.3.2: Stainless Steel

Stainless steel incorporates at least 12 wt. % chromium [54], which promotes the formation of a passive  $\text{Cr}_2\text{O}_3$  layer that can be stable in certain environments, but is dissolved by molten fluorides [50, 55, 56]. Work investigating the utilisation of stainless steels in molten salt reactors has not been actively pursued in over forty years, as work has focused primarily on nickel superalloys. As such, it is now appropriate to investigate materials such as modern stainless steels, which have progressed significantly over the last four decades. As previously stated, stainless steels showed a lower depth of attack when subjected to both static and dynamic testing, but Inconel was eventually used [46]. Recently numerous studies have investigated stainless steels in molten halide environments, with some promising results.

The most well-known family of stainless steels are austenitic ( $\gamma$ ), (300 series) with a face centred cubic structure, which show enhanced corrosion resistance compared to ferritic (body centred cubic) and martensitic (body centred tetragonal) steels [57]. Consequently, this investigation focuses primarily

on austenitic stainless steels. Austenitic stainless steel can have numerous different alloying additions, including but not limited to carbon and nitrogen, which act as austenite stabilisers reducing the requirement for nickel. Molybdenum, titanium and niobium can also increase corrosion resistance; molybdenum is present as a lone element, as are chromium and nickel. Whereas titanium and niobium form carbide precipitates, this reduces the formation of metal carbide precipitates at the grain boundaries. The presence of these precipitates leads to metal depletion at the grain boundaries, which can cause corrosive attack [54].

Static corrosion tests have been conducted on numerous stainless steels in the 300 and 400 series and it was found that the majority of the 300 (austenitic stainless steels) and 400 (ferritic and martensitic stainless steels) series samples tested showed a depth of attack of 1 mm or less, with the main form of corrosive attack being the formation of subsurface voids along with grain boundary attack leading to intergranular corrosion [46]. As previously mentioned, embrittlement via irradiation has been investigated by McCoy et al. [53]; it was discovered that Hastelloy N was embrittled, but stainless steel 304 showed no intergranular embrittlement [44].

It is evident that stainless steel had some highly advantageous properties for its use in a molten salt reactor, and with the many advancements that have been made it is highly likely that a stainless steel can be developed to rival nickel superalloys.

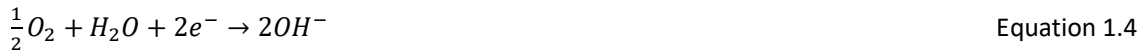
#### 1.4: Basic Principles of Corrosion

Usually, metallic corrosion involves the degradation of a material through an electrochemical reaction. Corrosion within a molten salt is complex when compared with aqueous corrosion, which has a much wider knowledge base, and involves moisture, oxygen and impurities within the system. Initially an aqueous environment will be reported on, and then a more in depth look at salt corrosion will be given in Section 1.5.

Corrosion consists of two electrochemical reactions, one anodic and the other cathodic. Oxidation is the anodic reaction and describes the process of metal dissolution, whereby a metal will lose one or more electrons and become positively charged, as shown in Equation 1.3 [56].



Reduction is the cathodic reaction and often occurs via Equation 1.4.



For corrosion to take place, a system requires an anode for metal degradation to take place, a cathode where oxygen is reduced to form negative ions, and a conductive electrolyte.

As both the anodic and cathodic reactions take place simultaneously to ensure the system is kept at equilibrium, Equation 1.3 and Equation 1.4 can be combined as shown in Equation 1.5 [58]. The positive metal ion will usually form a metal complex with the product from the cathodic reaction.



Corrosion is influenced by numerous different factors, including temperature gradients, which within a dynamic system can lead to deposits of material, pH, surface quality and composition of the metal [59].

Stainless steel naturally forms a corrosion resistant layer, called a passivating layer. Chromium is added to the steel, and in the presence of air a thin inert chromium oxide layer is formed, which subsequently protects the steel from corrosive attack [60].

Corrosion takes place via a variety of different mechanisms, including, but not limited to, uniform attack, pitting, galvanic, crevice, stress and intergranular [61, 62]. It is believed that the predominant forms of corrosion in this work will be: pitting, due to the presence of chlorides which will act as a fluxing agent; uniform, as the whole sample will be in full contact with the molten salt throughout the experiment, and intergranular, which is a known form of selective attack, which takes place at the grain boundaries and has previously being reported by Richardson et al. [46].

Uniform corrosion takes place evenly over the whole of the metallic surface, and although it is the most common form of corrosion it is easy to predict and is therefore not deemed to be the most serious [63].

The process of intergranular corrosion focuses on corrosion where grain boundaries are preferentially attacked due to the depletion of the corrosion resistant alloys at the boundaries [60]. This is often observed in nickel alloys and austenitic stainless steel whereby chromium carbide is formed at the grain boundary, resulting in a depletion of the corrosion resistant chromium addition in the adjacent areas [60, 64].

Finally, pitting is a localised form of attack and occurs in alloys that have a passivating layer. It is widely cited as the most dangerous type of corrosion as it is difficult to detect and predict [62]. It is an autocatalytic process and occurs due to the breakdown of the passivating layer. When a small area of this layer becomes damaged, passivation is lost and the metal now acts as the anode, while some part of the surrounding area, which is still protected by the film, will serve as the cathode [65].

## 1.5: Materials Corrosion in Molten Salts

Chlorides and fluorides are generally considered stable in an inert atmosphere, but both can act as fluxing agents. Oxide layers, such as  $\text{Fe}_2\text{O}_3$ ,  $\text{Cr}_2\text{O}_3$  and  $\text{Al}_2\text{O}_3$  that often act to passivate alloys in an aqueous environment, dissolve in the molten salt, leading to an increased corrosion rate [36, 55, 56, 66].

Once the protective oxide layer is removed, corrosion of the most chemically reactive element will take place [67].

### *1.5.1: Fluoride Systems*

Chemical thermodynamics is one of the major driving forces behind corrosion in a molten salt, and the difference in the Gibbs free energy of formation for the fluoride salt and the metal fluoride can provide insight into the likelihood of a product forming. A complex with a more negative Gibbs free energy is more likely to materialise, and therefore alloying elements within the sample whose fluorides have a more negative Gibbs free energy of formation compared to the salt, will preferentially form these compounds. Table 1.1 gives some insight into the free energy of formation of some common salt constituents and alloying additions [36, 66].

Table 1.1: Gibbs free energy of formation for some common fluoride compounds utilised in nuclear systems at 727°C [36].

Fluoride compound	Gibbs free energy of formation, kJ/(mol·K)
LiF	-941.40
NaF	-843.49
KF	-820.90
BeF <sub>2</sub>	-783.24
ZrF <sub>4</sub>	-707.93
HF	-498.57
AlF <sub>3</sub>	-677.81
CrF <sub>2</sub>	-566.35
CrF <sub>3</sub>	-544.51
FeF <sub>2</sub>	-500.82
NiF <sub>2</sub>	-416.48

From Table 1.1, if a salt such as FLiNaK is used in a molten salt reactor, all of the salts that make up the molten salt system need to have a more negative free energy of formation compared to the fluorides of the structural material. Therefore, in a system with no impurities the alloy of construction and the salt should be in equilibrium, and once equilibrium is reached no corrosion should take place [36]. Generally to prevent corrosion it is advisable to keep the difference between the salt and the alloying additions more than 84 kJ/(mol·K) [20].

It has been noted by numerous authors [46, 50] that chromium appears to be the main corrosion resisting component within an alloy, this coincides with the Gibbs free energies seen in Table 1.1 as chromium complexes have the most negative free energy, implying that if corrosion of an alloy containing the elemental additions detailed in Table 1.1 were to take place, chromium would be attacked first if the alloy is homogenous [46, 51, 66, 68].

It has been indicated by numerous authors who have studied a range of nickel superalloys and stainless steels in a molten fluoride environment, that within a closed system, a steady corrosion rate is reached after 500 hours. Impurities within the system can cause a high initial rate of corrosion, but after 500 hours impurities have been consumed and the corrosion reaches a steady state lower than that observed at the beginning of the process [46, 69, 70].

Nishikata et al. [56] used electrochemical techniques to investigate metal corrosion by numerous molten salts. They highlighted that this technique is more accurate compared to other techniques, such as surface observations and gravimetric methods which are normally used in these investigations.

As mentioned in Section 1.4 the anodic reaction defines the dissolution of the metal, which is the same in both an aqueous and molten salt system. The cathodic reaction is generally due to contaminants within the system and therefore can be more complex to identify. Contaminants such as O<sub>2</sub>, H<sup>+</sup>, H<sub>2</sub>O and OH<sup>-</sup> are usually responsible for corrosion, and the two main contributors to corrosion within a molten salt are water and oxygen. Nishikata defined the cathodic reactions that take place within the system and these are shown in Equation 1.6-Equation 1.10 [56].

Reaction with water and without oxygen



Reaction with oxygen and without water



Reaction with water in the presence of oxygen



It is possible for a one step reaction to take place in the presence of both water and oxygen via Equation 1.11



Further corrosion mechanisms have been proposed by Ouyang et al. [71] for metal alloys within a molten fluoride due to the presence of impurities (Equation 1.12-Equation 1.14).



Where A represents an alkali metal such as lithium, potassium or sodium [71]. The metal cation, once formed from the oxidation of a metal (anodic reaction), can react with molten salt components or any of the charged species formed in the cathodic reaction to form a metal complex.

Hydrogen can also be formed when water or HF reacts with the alloying elements (denoted as M) and oxides of the cation part of the salts via the following reactions, Equation 1.16-Equation 1.18 [36].



The above reactions will lead to an excess of oxides and metal fluorides of the alloying elements.

These metallic impurities can react further with alloying constituents leading to a more aggressive attack, and it has been observed that the deliberate addition of iron fluoride into the salt can result in a higher corrosion rate via Equation 1.20 [36].



Oxides on the surface can leach out chromium, an essential alloying constituent preventing air side corrosion, via the following reaction [36].



Finally, chromium can also be leached directly via the fuel salt  $UF_4$  via Equation 1.22.



Further work by Olson [50] found that moisture can react with a molten alkali fluoride (AF), via Equation 1.23 and Equation 1.24, to form corrosive hydrofluoric acid, HF.



Electrochemical techniques were used [51] to determine the dissolution rate of numerous elements within an LiF-NaF melt, and it was found that thermochemical calculations were difficult to conduct, but electrochemical techniques allowed the determination of the reactivity and kinetics. It was concluded that the metal stability of the elements tested increased in the following order: chromium, iron, nickel, molybdenum, tungsten, silver and gold. This paper also highlights that the reaction rate for chromium and iron is controlled by the metal-salt interface and not diffusion [51]. Similar work by NASA investigating the elements in the single salts that make up FLiNaK found via equilibrium concentrations that the tendency of an element to be attacked increased in the order nickel, cobalt, iron, chromium and aluminium. It was also concluded that potassium chloride is more corrosive than lithium chloride [36].

Thermal gradient-driven corrosion is also an important part of the corrosion of structural materials with fluorides, and it was possible to investigate this over the operational life of the MSRE. The solubility of the corrosion products depends on the temperature of the system. The corrosion products formed in the hot area of the loop (700°C) can deposit in the cooler areas (560°C), and so the driving force for the mass transfer of the corrosion products is the temperature gradient in the system. It was observed that the cooler areas become a sink for the corrosion products and large deposits of material were seen, while voids up to 50 µm below the surface were present in the hot section, meaning that more corrosion has occurred in the hot leg [72]. A mechanism has been proposed for this system, which indicates that removal of the alloy constituent in the hot section increases to a point where its concentration on the cooler side reaches the saturation limit in the salt. This in turn leads to nucleation as a solid in the cool section of the system, resulting in a build-up of corrosion products in the cold leg, which can diffuse into the bulk material. This is particularly important when molten salts are used as a coolant, where corrosion from the hot section can lead to blockages in the cooler sections [36, 73].

Corrosion can also be accelerated by activity gradients, whereby two different materials in the same vicinity as one another in a molten salt can increase corrosion. Species dissolved into the molten salt with a higher activity can deposit on a material with a lower activity. This is observed in Hastelloy N in the presence of Alloy-25 which is rich in cobalt; when placed in the same vicinity as each other, cobalt deposits onto Hastelloy N [74]. This type of corrosion can be particularly pronounced if one of the materials has an affinity for the dissolved species and can form a thermodynamically favourable compound, and these issues are more pronounced in static corrosion tests [74].

This was observed in work conducted by Olson et al. [50] whereby seven different alloys were tested in molten FLiNaK contained within a graphite crucible. It was discovered that there is a correlation between the chromium content of the alloy and corrosion, but this analysis was only valid when the chromium content of the alloys was between 20-23 wt. %, as there appears to be a correlation between the carbon and chromium content in the alloy. It was suggested that chromium carbide forms on the surface, and it was found via cross sectional SEM images of the graphite crucible that chromium migrated to the surface of the crucible and formed chromium carbide. Further tests did confirm that the formation of chromium carbide was due to the dissimilar materials, but the mechanism for reaction did not change significantly [52].

### 1.5.2: Chloride Systems

The majority of work into corrosion of molten halides for use as a primary coolant in nuclear systems has focused on fluorides, as chlorides require isotopic separation to avoid the high neutron cross section and waste management associated with chlorine-36 [75]. Alkali and alkaline earth chlorides are more thermodynamically favourable than transition metal chlorides, and it is proposed that corrosion should not occur when structural alloys are in contact with molten chlorides. Therefore, the corrosion within a molten chloride is driven by the presence of impurities [36]. Chloride ions can act as fluxing agents. In chloride salts the formation of an oxide is favoured thermodynamically although the ability to form is difficult, but passivity is observed. An example of this is the corrosion of Hastelloy X, a nickel based superalloy, in  $\text{NdCl}_3\text{-NaCl-KCl}$  at 550, 600 and 800°C; it was found that the nickel oxide present on the surface of the alloy can react with  $\text{NdCl}_3$  (neodymium (III) chloride) to form neodymium oxychloride via Equation 1.24-Equation 1.26.



Further to these reactions, any moisture within the system can react via Equation 1.27.



Alloying constituents can react with hydrochloric acid formed in Equation 1.27 and become chlorinated, as shown in Equation 1.28.



An example of this is shown in Equation 1.29.



Chromium is the more readily attacked metal, with alloys that have similar compositions showing an increase in the rate of corrosion in the presence of carbon, but addition of metals that will readily form carbides such as niobium and titanium can reduce corrosion [36].

An investigation by Ambrosek [77] into corrosion in molten  $\text{KCl-MgCl}_2$  for a variety of high temperature nickel alloys and stainless steel 316L showed preferential attack on chromium, with corrosion taking place predominantly at the grain boundaries. It was found that the nickel alloys were less resistant to

corrosive attack in the chloride salt compared to FLiNaK, believed to be due to the preferential formation of nickel chlorides [36].

Further work on corrosion in molten chlorides by Ozeryanaya [78] has shown that testing low carbon steels in a variety of environments at 900°C in molten KCl yields different results. For example, the corrosion rate increased by a factor of 4 when the reaction was conducted in air, and experiments covered in HCl increased by a factor of 10 [78].

Testing of corrosion of materials that could be used in a molten salt reactor within a molten chloride has not been as thoroughly researched as fluoride salts. Despite this it is believed that chloride will behave in a comparable way to fluorides.

## 1.6: Studies of Corrosion of Different Alloys in Molten Salts

As previously mentioned, nickel superalloys have been used in the two experimental reactors built by ORNL, therefore a lot of work has investigated nickel superalloy corrosion within molten salts. Work into stainless steel has not been as thorough, but recent research has started to investigate the behaviour of stainless steel within a molten salt environment.

### *1.6.1: Nickel Superalloys*

Corrosion of a material can be heightened by the presence of impurities in the salt, this was discussed in Section 1.5. The effect of moisture within a molten salt on the corrosion rate was investigated by Ouyang et al. [71], four alloys were tested in a FLiNaK (LiF-NaF-KF (lithium fluoride-sodium fluoride-potassium fluoride)) salt mixture at 600-700°C for 100-200 hours. The compositions of the four alloys are shown in the Appendix, Table A.2. Figure 1.4 shows the resultant samples after immersion for 100 and 200 hours at moisture contents of 1.91 and 3.19 wt. % [71].

It was discovered that chromium content alone does not dictate the corrosion of the alloys. Similar mass losses were observed for Hastelloy N and B3, where the chromium contents of these alloys are 7 and 1.5 wt. % respectively. A higher mass loss was seen for Haynes-242 (chromium content 8 wt. %) compared to Hastelloy N. Ouyang et al. concluded that molybdenum content contributes to corrosion if moisture is present in the system. Further work on a high molybdenum alloy, TZM, showed a substantial mass loss, confirming the previously postulated theory [71].

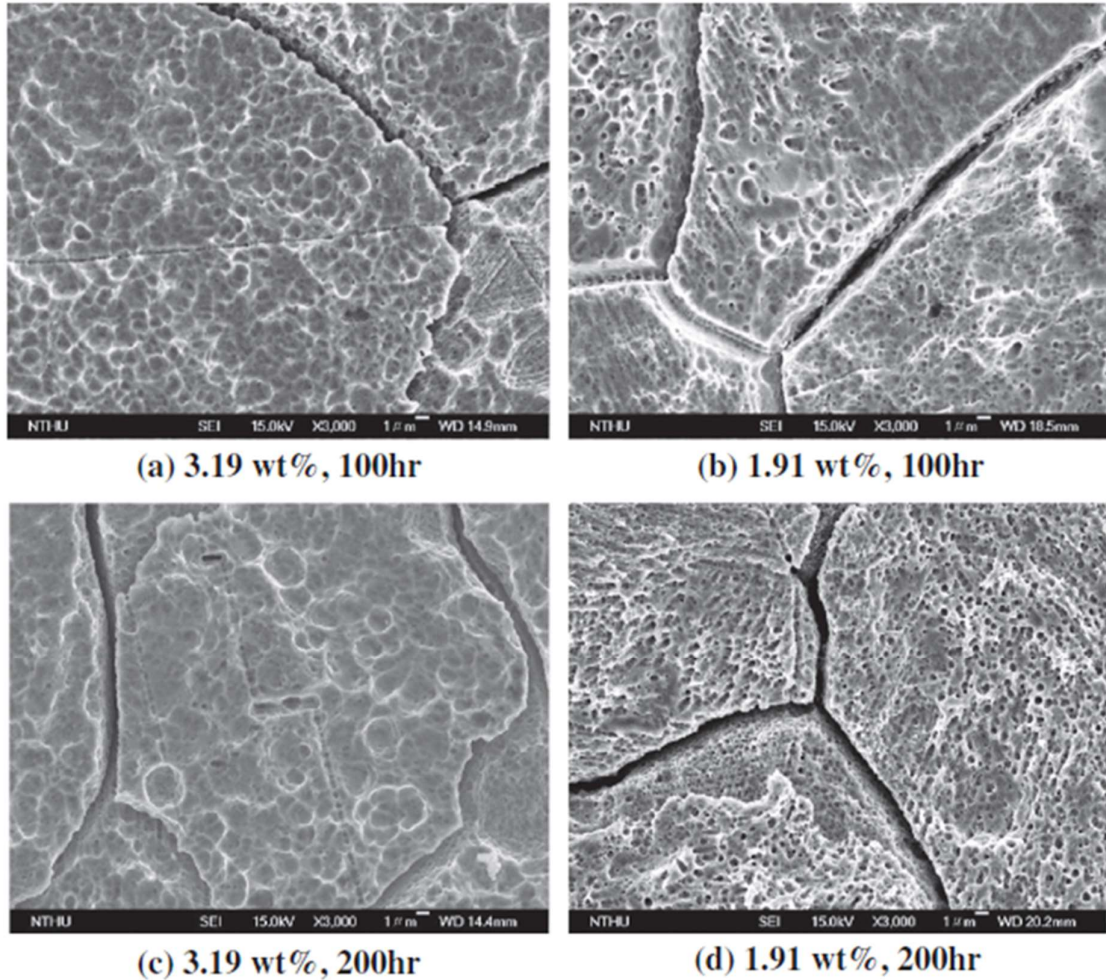


Figure 1.4: SEM images obtained by Ouyang et al. showing the morphology of Hastelloy N after immersion in FLiNaK at 700°C with different moisture contents as indicated [71].

Ouyang's previous work investigated corrosion using a purified salt, and corrosion was substantially (25 times) lower, even when tests were run at higher temperatures (850°C) and for longer periods (500 hours) [71].

In 1969, Devan [69] investigated the effect of different alloying additions in a nickel-molybdenum alloy in contact with fluoride melts. Seven different elements; vanadium, niobium, titanium, aluminium, tungsten, iron and chromium, were added to a nickel molybdenum alloy containing 17 wt. % molybdenum and placed in a NaF-LiF-KF-UF<sub>4</sub> (11.2-41-45.3-2.5 mol.%) salt mixture. It was found that the concentration of the corrosion product increased with increasing amounts of iron, niobium, vanadium, chromium, titanium and aluminium respectively. Devan concluded that there is substantial choice when proposing alloying additions as long as titanium and aluminium are avoided, especially when used in combination or instead of chromium [69].

Olsen et al. investigated seven different alloys in a FLiNaK salt mixture, their compositions are given in the Appendix, Table A.3 [50]. Olsen et al. [50] found that Inconel 617, which has a similar composition to Hastelloy X, had almost double the weight loss when the two alloys were compared. This was ascribed to the iron in Hastelloy X being replaced by cobalt in Inconel 617, suggesting that chromium is not the only problematic addition, this was seen by Ouyang et al. and by Devan [69, 71]. This work further confirmed that molybdenum and nickel both show a strong corrosion resistance, which has been seen in previous work [9, 16, 26], and that tungsten also shows good corrosion resistance [50].

Recent work undertaken at the Kurchatov Institute [79] investigated nickel molybdenum alloys in molten fluorides, and concluded that reducing titanium content to below 0.5 wt. % and an aluminium content of 2.5 wt. % gave a significantly reduced corrosion rate. Approximately seventy different compositions were tested, with the results suggesting that addition of titanium, aluminium and vanadium gave the best properties, and it was proposed that aluminium can increase the high temperature strength. Therefore, it may be possible to replace some of the chromium within the system [79].

Research has also been undertaken on the behaviour of nickel superalloys in chlorides. Three different nickel superalloys, Hastelloy C-276, Hastelloy C-22 and Hastelloy N, whose compositions are given in the Appendix, Table A.4, were tested in a molten chloride mixture of NaCl-KCl-ZnCl<sub>2</sub> (sodium chloride-potassium chloride-zinc chloride). It was concluded by Vignarooban et al. [80] that C-276 gave the lowest corrosion rate and Hastelloy N gave the highest. It was theorised by the authors that this was due to the high chromium content in Hastelloy C-276 and C22 compared to Hastelloy N. However, it is also possible that silicon reduces corrosion resistance, as ten times more silicon is present in Hastelloy N compared to the two other alloys [80].

Further work investigated three different superalloys, their compositions are given in the Appendix, Table A.5, in a LiCl-Li<sub>2</sub>O (lithium chloride-lithium oxide) molten salt at 675°C in an oxidising environment for 72 and 216 hours, and showed that the different elemental compositions resulted in different corrosion products [81].

Incoloy 713LC showed the lowest corrosion rate among these alloys, with the authors postulating that the presence of a surface corrosion layer acting as a protective layer may reduce ingress of the corrosive salt. Cross sectional SEM/EDX showed a dense corrosion layer, made up of two layers. The outer layer consisted of nickel and chromium oxides, believed to be a Ni-Cr spinel, NiCr<sub>2</sub>O<sub>4</sub>, formed by a reaction between surface NiO and Cr<sub>2</sub>O<sub>3</sub>. The inner layer was comprised of oxygen active elements

such as aluminium and titanium [81]. The corrosion products detected by XRD for each of the samples are shown in Table 1.2.

*Table 1.2: Corrosion products seen on the surface of each of the alloy samples investigated by Cho et al. [81].*

	72 hours	216 hours
Inconel 713LC	Cr <sub>2</sub> O <sub>3</sub> , NiCr <sub>2</sub> O <sub>4</sub> , NiO	Cr <sub>2</sub> O <sub>3</sub> , NiCr <sub>2</sub> O <sub>4</sub> , NiO
Nimonic 80A	Cr <sub>2</sub> O <sub>3</sub> , LiFeO <sub>2</sub>	(Cr, Ti) <sub>2</sub> O <sub>3</sub> , Li <sub>2</sub> Ni <sub>8</sub> O <sub>10</sub>
Nimonic 90	Cr <sub>2</sub> O <sub>3</sub> , CoCr <sub>2</sub> O <sub>4</sub>	CoCr <sub>2</sub> O <sub>4</sub> , (Cr,Ti) <sub>2</sub> O <sub>3</sub> , LiAlO <sub>2</sub>

After 72 hours chromium rich corrosion products were observed on all three alloys, due to the high thermodynamic stability of Cr<sub>2</sub>O<sub>3</sub>. Each of the alloys then forms different corrosion products dependent on their elemental compositions. Both Nimonic 80A and 90 form chromium titanium oxides, due to the high wt. % of titanium present within each of the alloys. The formation of LiFeO<sub>2</sub> is believed to be due to the high diffusion coefficient and wt. % of iron in Nimonic 80A.

It was also found that higher chromium concentration enhanced uniform corrosion of the samples, both Nimonic 80A and Nimonic 90 showed uniform corrosion, whereas localised corrosion was found on Inconel 713LC. However, this work also suggests that too high a concentration of chromium can be deleterious to corrosion resistance as spalling can occur, which in turn leads to the depletion of chromium in the corrosion layer [81].

### *1.6.2: Stainless Steel*

Initial work by ORNL in 1953 investigated corrosion by molten fluorides via dynamic and static tests on primarily nickel superalloys, and these were discussed in Section 1.3.1. Static corrosion tests also took place on numerous stainless steels in the 300 and 400 series, and it was found that the majority of the 300 (austenitic stainless steels) and 400 (ferritic and martensitic stainless steels) series samples tested showed a depth of attack of 1 mm or less, with the main form of corrosive attack being the formation of subsurface voids along with grain boundary attack leading to intergranular corrosion [46].

An investigation into the compatibility of stainless steel 316 with FLiBe for use in a fusion reactor was published by ORNL in 1979. A test loop incorporating both hot and cold regions was used in a dynamic test. The maximum temperature of the hot area was 650°C and the maximum temperature difference observed was 125°C. It was found that corrosion products were removed from the hot leg and deposited on the cold leg (this is normally observed in dynamic testing with temperature differences). Within the first 1000 hours the corrosion rate was relatively rapid with subsequent decrease in the

second 1000 hours [82]. This is similar to previously reported work [46, 56, 69, 70]. The average corrosion rate between 3000-9000 hours was 8  $\mu\text{m}/\text{year}$ . This work also highlighted the dependence of chromium content on corrosion rate: within the first 3000 hours the chromium concentration within the salt increased to 400 wt. ppm, which is ten times the original value. In comparison, the iron and nickel contents remained relatively consistent [82].

Tortorelli et al. investigated stainless steel 316 in a molten LiF-LiCl-LiBr (lithium fluoride-lithium chloride-lithium bromide) environment. The samples withstood temperatures of 500°C for 2675 hours with a relatively low corrosion rate with a depth of attack of 1-1.8  $\mu\text{m}$  [83].

Shinata et al. investigated the corrosion of four different steels, whose compositions and structural types are shown in the Appendix, Table A.6, in sodium chloride (NaCl) at a range of temperatures between 650 and 900°C; it was found that the rate of corrosion increased considerably above the melting temperature of NaCl, 801°C [84]. As mentioned previously chromium is selectively oxidised to form a  $\text{Cr}_2\text{O}_3$  passivating layer, therefore corrosion is significantly increased in samples containing a higher chromium content. Nickel within stainless steels can restrict the oxidation of chromium, and therefore the ferrite stainless steels showed a higher corrosion rate due to their high chromium and low nickel content [85].

It was also determined from analysis of stainless steels 430 and 316 that nickel would also be preferentially oxidised, but only above the melting temperature of sodium chloride (NaCl) [85].

Hiramatsu et al. continued this work and investigated the effects of different alloying elements on stainless steels in hot sodium chloride below its melting point using a cyclic heating system. Nine different stainless steels were studied and the work investigating the difference in corrosion between ferritic and austenitic stainless steels previously done by Shinata et al. was confirmed. Hiramatsu et al. found that the addition of silicon to austenitic stainless steels showed the best corrosion resistance, this is believed to be due to the formation of silicon oxide within the steel, which has good heat resistance properties. The silicon oxide is believed to form near the surface or along the grain boundaries and resists reactions with sodium chloride (NaCl). Finally, it was concluded that corrosion increased when chromium oxide ( $\text{Cr}_2\text{O}_3$ ) and aluminium oxide ( $\text{Al}_2\text{O}_3$ ) are present as they react with NaCl and form a spinel oxide, such as  $\text{Na}_2\text{CrO}_4$ , rather than the protective oxide layer which is often seen in stainless steel. The formation of  $\text{Na}_2\text{CrO}_4$  leads to generation of free chlorine which can readily react with chromium in the steel, giving rise to volatile  $\text{CrCl}_3$ . Therefore, the protection normally attributed to chromium is lost and iron and other metals are more readily chlorinated and oxidised. This was confirmed by the presence of iron oxides in the XRD (X-ray diffraction) pattern [86].

Further work of this nature was conducted by Polovov et al. [87] who examined the corrosion rate of three different stainless steels in a NaCl-KCl mixture at 750°C. The compositions of the three steels are shown in the Appendix, Table A.7.

Polovov et al. [87] indicated that these three steels were chosen as they show enhanced capabilities in a molten salt environment. SS316L shows enhanced resistance against chloride pitting, a localised form of corrosion, which results in shallow holes on the surface [54]. SS321 has high heat resistance up to 850°C and 316Ti shows sensitisation resistance, where sensitisation refers to the depletion of chromium at the grain boundary due to the formation of chromium carbide precipitates [87]. Polovov et al. determined that all three alloys showed a low corrosion rate as determined by weight loss. It was also determined via metallographic analysis that a common corrosion mechanism, gradual etching followed by intergranular corrosion, was occurring on all three alloys. Stainless steel 316L showed the lowest corrosion rate and this was ascribed to its low carbon content. It was proposed that stainless steel corrosion takes place due to a chemical exchange reaction between the salt and the metal where a large difference in redox potentials leads to a higher rate of corrosion, eventually these potentials decrease along with the corrosion rate [87]. A similar mechanism is also seen in nickel superalloys, where after 500 hours the corrosion rate decreases [46, 56, 69].

Shankar and Mudali [88] investigated stainless steel 316L, and also stainless steel 316L coated with yttria-stabilised zirconia in molten LiCl-KCl, for use in pyrochemical reprocessing. The samples were tested at 600°C and the uncoated stainless steel held for 25, 100 and 250 hours whereas the coated sample were held for 1000 hours. The uncoated sample had a percentage weight loss between 0.3 and 2.83% for a maximum exposure time of 250 hours, whereas the coated sample showed a percentage weight loss of 0.08% for 1000 hours, clearly showing that corrosive attack is more prevalent in the uncoated sample. Scanning electron microscopy (SEM) and EDX (energy-dispersive X-ray spectroscopy) analysis of the uncoated stainless steel showed that the corrosion product was chromium rich and had a porous surface, with increasing pore size as exposure time increased, whereas areas where the corrosion product had not formed were rich in iron and nickel and depleted in chromium. This work indicates that chromium is selectively leached from the surface to form the corrosion product. As expected, longer exposure times led to a thicker degradation layer, and spalling was more pronounced in the sample that was immersed for 250 hours. Cross sectional SEM of the samples revealed three different layers: the surface layer with a chromium rich compound present, the second inner layer containing pores which are enriched with nickel and iron, whilst depleted in chromium; and finally the inner layer is the unaffected substrate. Images from the surface, using SEM, of the yttria stabilised zirconia coated stainless steel 316L before and after immersion show little

difference in their structure. Further cross sectional analysis did not show any selective leaching of elements [88].

Work by Sellers et al. [89] in 2014 investigated static corrosion of nine different alloys in a molten FLiNaK eutectic at 850°C in a controlled environment. The samples were sealed into stainless steel crucibles, but due to a leak from one of the crucibles a chemical reaction took place between the molten salt and the furnace insulation, made up of clay bonded silicon carbide. This released corrosive vapours of  $\text{Na}_2\text{SiF}_6$ ,  $\text{K}_2\text{SiF}_6$ ,  $\text{SiF}_3$  and  $\text{F}_2$ , which subsequently reacted with the stainless steel crucibles causing the molten salt to leak further, forming more vapour, causing further reactions with the stainless steel and the cycle continued. It was stated that oxygen ingress was highly unlikely within the system as a nitrogen cover gas was used in the furnace. As the initial aim of this experiment was not to investigate the corrosion mechanism in the event of a failure it was difficult for the authors to identify the corrosion mechanism, although it was postulated that a failure due to a weld point led to the release of the salt, resulting in outward corrosion of the crucible leading to stress induced cracking, could be a method for this attack. An image of the crucibles before and after the experiment is shown in Figure 1.5 [89].

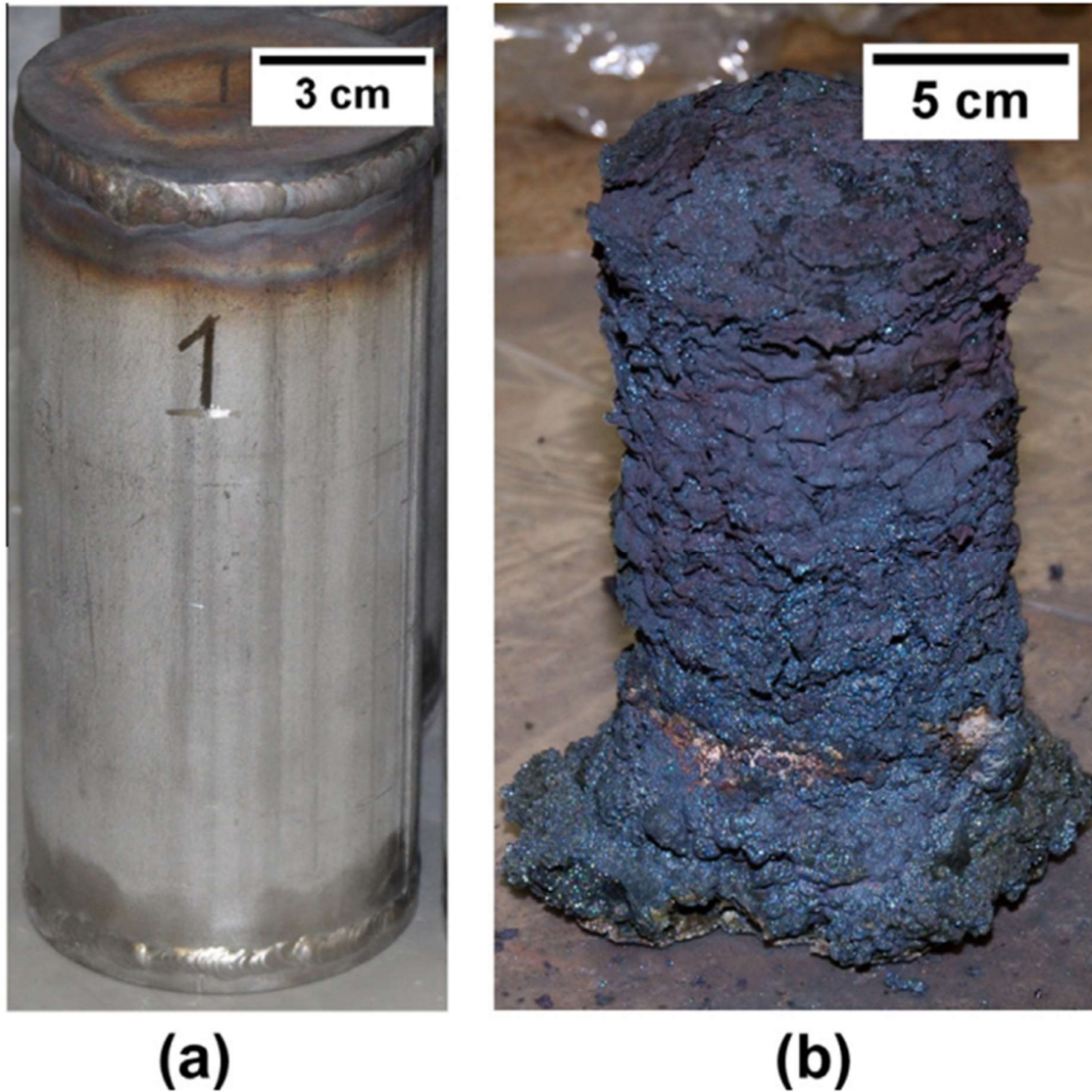
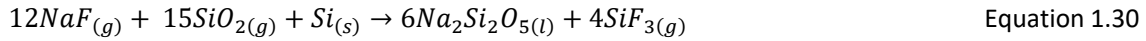
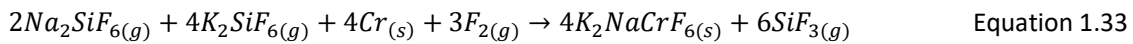


*Figure 1.5: Comparison of two stainless steel crucibles: (a) before testing, and (b) after testing in a molten FLiNaK eutectic at 850°C. Note the difference in scale, there has been substantial growth in the height and width of the crucible due to the corrosion products [89].*

The corrosion product, which via visual inspection was porous and brittle, was analysed further using SEM/EDX and XRD. Numerous different corrosion products were observed in the EDX analysis and it was found that within the rough edges there was an abundance of oxygen, silicon, potassium and iron, and within these sections there were areas rich with iron and oxygen, identified as hematite ( $\text{Fe}_2\text{O}_3$ ). In addition to this, smoother sections which contain potassium, oxygen and chromium were also observed. XRD analysis confirms the presence of  $\text{K}_2\text{NaCrF}_6$ . Finally a hypothesis was proposed for the formation of the porous and brittle corrosion product, as outlined in Equation 1.30-Equation 1.32, where M is a metal element, usually iron, chromium or nickel.



It was believed that due to the presence of silicon and silicon oxide within the furnace insulation and also the presence of sodium fluoride within the system it was highly likely that the above equations took place. Further to this a hypothesis for the formation of  $K_2NaCrF_6$  is also proposed (Equation 1.33), it is believed that a similar reaction (Equation 1.30) can take place, but with potassium chloride (KF) instead of sodium fluoride (NaF), which would lead to the formation of  $K_2SiF_6$ .



As chromium and iron are the more thermodynamically favourable elements to be leached out of an alloy in the event of fluoride attack, it seems likely that chromium within the system will react with the sample. The porosity of the corrosion product is believed to be due to the sublimation of iron (II) fluoride, which can occur at temperatures as low as 690°C. This would lead to the expansion and eventual release of iron fluoride gas causing the porosity, which is seen in the corrosion product [89].

Further work into the corrosion resistance of stainless steel in molten salts has included super austenitic stainless steels. Due to their high nickel content and the added molybdenum they have shown improved corrosion resistance [60].

Five different Cr-Mo stainless steels with varying chromium content (compositions in the Appendix, Table A.8) were investigated at 550°C for 250, 500 and 1000 hours in a eutectic mixture of nitrates,  $LiNO_3$ ,  $NaNO_3$  and  $KNO_3$  [48]. It was discovered that corrosion was not only dependent on the oxidation, but also on "lithiumisation". It was found that addition of up to 9 wt. % chromium, increased corrosion resistance of the stainless steel.

The X-ray diffraction patterns for three of the samples showed  $LiFeO_2$  to be present on the outer oxide layer, adopting three different crystal structures, rhombohedral, cubic and tetragonal. The inner oxide layer was identified as  $(Fe, Cr)_3O_4$ . Lithium cannot easily be identified by SEM/EDX due to its low atomic number, however SEM/EDX shows the presence of chromium and iron in the inner layer and just iron in the outer layer. Cheng concluded that as  $LiNO_3$  is more basic than  $NaNO_3$  and  $KNO_3$ , the stainless steels were attacked via an oxidative route and also by the lithium present in the salt [48].

Kruizenga and Gill [90] investigated two stainless steels whose compositions are given in the Appendix, Table A.9, with similar compositions except that they are stabilised by two different elements: 321SS

is stabilised by titanium and 347SS is stabilised by niobium. Tests were performed at 400, 500, 600 and 680°C for up to 3000 hours.

It was found that the corrosion rate of 347SS was 30-40% lower than that seen in 321SS. The main corrosion product formed on 347SS is  $\text{Cr}_2\text{O}_3$  whereas the main corrosion product formed by 321SS is iron oxide on the outermost layer, evolving to a mixed chromium iron oxide deeper in the sample. Surface spalling was also reported at high temperatures in 321SS [90].

At 500°C it was shown that the corrosion products were primarily iron oxide on the outer surface and iron and chromium on the inner surface, whereas above 600°C the outer layer contained both iron oxide and sodium ferrite, while mixed oxides were present in the inner layer [90].

Highly alloyed stainless steel (AVESTA 254 SMO) containing 6 wt. % molybdenum, and two stainless steels (316L and alloy 904L), were tested for use in a desalination facility, their compositions are given in the Appendix, Table A.10. Water at a temperature between 17-36°C with a chloride content of 25,000 ppm, and natural sea water, were investigated. It was found that AVESTA 254 SMO showed no crevice cracking, which is normally seen after 17 months in stainless steel 316L. Corrosion of 904L and 316 is usually observed after 18 months in natural seawater, but this was not seen even after 40 months for AVESTA 254 SMO [91].

These experiments were undertaken at low temperatures; no published work was discovered that investigated these alloys at the temperatures experienced in a molten salt reactor. As low corrosion rates are seen at low temperatures after 40 months, it is envisioned that stainless steels are ripe for further investigation [91].

Further work investigated the corrosion resistance of AVESTA 654 SMO compared to stainless steels 316L and AVESTA 254, along with a duplex stainless steel (AVESTA SAF 2504) and two nickel superalloys, alloy 625 and C276, whose compositions are given in the Appendix, Table A.11 [92].

Each alloy was tested in three different solutions,  $\text{FeCl}_3$ ,  $\text{FeCl}_3\text{-CuCl}_2\text{-NaCl-H}_2\text{SO}_4\text{-HCl}$  and  $\text{Fe}_2(\text{SO}_4)_3\text{-NaCl-HCl}$ . It was found that AVESTA 654 SMO showed enhanced corrosion resistance when compared to the other stainless steels and alloy 625 [92].

An extensive study by Malik et al. [93] investigated the corrosion behaviour of fifteen different stainless steels, including austenitic, ferritic, super austenitic, super ferritic and duplex types, in seawater at 50°C. They found that chromium, molybdenum and nitrogen impact the corrosion rate of stainless steel and adjusting their composition within an alloy can give a corrosion rate lower than that observed for stainless steel 316 in seawater. It was also discovered that in highly alloyed steels it took a longer time for pitting to occur (20-40 hours) compared to conventional steels (4-14 hours) [93].

An optimised super austenitic stainless steel, 27-7MO whose composition is in the Appendix, Table A.12, was developed by Muro et al. [94], and was shown to have excellent mechanical properties and corrosion resistance when compared to nickel superalloys. Tests were conducted both in boiling magnesium chloride solution and in seawater, where 27-7MO showed excellent resistance to stress corrosion cracking induced by chlorides. The high chromium and molybdenum content of this alloy is believed to be responsible for the enhanced corrosion resistance, and combining nickel and nitrogen gives some protection against secondary phases [94].

## 1.7: Key Gaps in Understanding

The majority of previous work has focused primarily on corrosion of nickel superalloys within a molten salt as historically this has been the preferred material of construction. It is proposed that as there have been substantial improvements in the properties of stainless steel over the past forty years, it is possible that modern stainless steels can be utilised as a material of construction for molten salt reactors.

### 1.7.1: Aims

The aim of this project is to investigate the corrosion of stainless steel samples within a molten chloride salt.

### 1.7.2: Objectives

1. Corrode stainless steel 316L samples in a ternary alkali chloride salt (LiCl-KCl-NaCl) and examine the samples via SEM and XRD
2. Investigate the effect of lithium on the samples by comparing stainless steel 316L corroded in a ternary and a binary eutectic salt (LiCl-KCl-NaCl and NaCl-KCl) and examine via SEM and XRD.
3. Using stainless steel 316L as a baseline, investigate different compositions of stainless steel along with iron in a ternary alkali chloride salt, and examine via SEM and XRD
4. The effect of time is also investigated with each sample being examined over multiple time scales.

### Literature cited

1. International Atomic Energy Agency (IAEA), *2015 Key World Energy Statistics*, Economic Co-operation and Development (OECD). 2015, International Energy Agency
2. World Energy Council, *Deciding the Future: Energy policy Scenarios to 2050. Executive Summary*. 2007.
3. International Energy Agency, *IEA says push for renewables and nuclear power is coherent with Finland's long-term decarbonisation strategy*, Press Releases May 2013.
4. *A Technology Roadmap for Generation IV Nuclear Energy Systems*. 2002, U.S DOE Nuclear Energy Research Advisory Committee, Generation IV International Forum.

5. *GIF R&D Outlook for Generation IV Nuclear Energy Systems* 2009, U.S DOE Nuclear Energy Research Committee, Generation IV International Forum.
6. S. Delpech, *Molten Salts for Nuclear Applications* in *Molten Salts Chemistry. From Lab to Applications*, F. Lantelme and H. Groult, Editors. 2013, Elsevier.
7. R.W. Moir, *Recommendations for a restart of molten salt reactor development*. *Energy Conversion and Management*, 2008. **49**(7): p. 1849-1858.
8. J. Uhlíř, *Chemistry and technology of Molten Salt Reactors – history and perspectives*. *Journal of Nuclear Materials*, 2007. **360**(1): p. 6-11.
9. C.W. Forsberg, *Thermal- and Fast-Spectrum Molten Salt Reactors for Actinide Burning and Fuel Production*, in *Advanced Nuclear Fuel Cycles and Systems*, Oak Ridge National Laboratory, Editor. 2007: Boise, Idaho.
10. J. Křepel, B. Hombourger, C. Fiorina, K. Mikityuk, U. Rohde, S. Kliem, and A. Pautz, *Fuel cycle advantages and dynamics features of liquid fueled MSR*. *Annals of Nuclear Energy*, 2014. **64**: p. 380-397.
11. R.W. Moir, *Cost of electricity from Molten Salt Reactors (MSR)* *Nuclear Technology*, 2002. **138**: p. 93-95.
12. H.G. MacPherson, *The Molten Salt Adventure*. *Nuclear Science and Engineering* 1985. **90**: p. 374-380.
13. C. Le Brun, L. Mathieu, D. Heuer, and A. Nuttin. *Impact of the MSBR concept technology on long-lived radio-toxicity and proliferation resistance*. in *Technical Meeting on Fissile Material Management Strategies for Sustainable Nuclear Energy*. 2005. Vienna, Austria: IAEA.
14. J. Kang and F.N. Von-Hippel, *U-232 and the Proliferation Resistance of U-233 in Spent Fuel*. *Science and Global Security*, 2001. **9**: p. 1-32.
15. D.J. Wilson, *The use of thorium as an alternative nuclear fuel*. 1982, Australian Atomic Energy Commission Research Establishment: Lucas Heights Research Laboratories
16. D. LeBlanc, *Molten salt reactors: A new beginning for an old idea*. *Nuclear Engineering and Design*, 2010. **240**(6): p. 1644-1656.
17. J. Serp, M. Allibert, O. Beneš, S. Delpech, O. Feynberg, V. Ghetta, D. Heuer, D. Holcomb, V. Ignatiev, J.L. Kloosterman, L. Luzzi, E. Merle-Lucotte, J. Uhlíř, R. Yoshioka, and D. Zhimin, *The molten salt reactor (MSR) in generation IV: Overview and perspectives*. *Progress in Nuclear Energy*, 2014. **77**: p. 308-319.
18. C.W. Forsberg. *Molten Salt Reactor Technology Gaps*. in *International Congress on the Advances in Nuclear Power Plants (ICAPP '06)*. 2006. Reno, Nevada.
19. S.R. Hill, P.C.G. Hodge, and T. Gibbs. *The potential of the molten salt reactor for warship propulsion*. in *Proceedings of the IMarEst 11th International Naval Engineering Conference and Exhibition, Parallel session G (Ship Design), paper 3*. 2012. London UK: BMT Defence Services Ltd, UK.
20. C.w. Forsberg. *Reactors with Molten Salts: Options and Missions*. in *Frederic Joliot & Otto Han Summer School on Nuclear Reactors "Physics, Fuels, and Systems"* 2004. Cadarache, France.
21. Christian Le Brun, *Molten Salts and nuclear energy production*. *Journal of Nuclear Materials*, 2007. **360**: p. 1-5.
22. M.W. Rosenthal, P.R. Kastan, and R.B. Briggs, *Molten Salt Reactors- History, Status and Potential*. 1969, Oak Ridge National Laboratory.
23. Generation IV International Forum, *Technology Roadmap Update for Generation IV Nuclear Energy Systems*. 2014, U.S DOE Nuclear Energy Research Advisory Committee.
24. H.A. Schmutz, P. Sabharwall, and C. Stoots, *Tritium Formation and Mitigation in High Temperature Reactors* 2012, Idaho National Laboratory.
25. A.M. Bradshaw, T. Hamacher, and U. Fischer, *Is nuclear fusion a sustainable energy form?* *Fusion Engineering and Design*, 2011. **86**(9–11): p. 2770-2773.

26. W.B. Cottrell, *Reactor Program of the Aircraft Nuclear Propulsion Project*. 1952: Oak Ridge National Laboratory
27. W.K Ergen, A.D Callihan, C.B. Mills, and Dunlap Scott, *The Aircraft Reactor Experiment-Physics*. Nuclear Science and Engineering, 1957. **2**(6): p. 826-840.
28. E.S. Bettis, W.B. Cottrell, E.R. Mann, J.L. Meem, and G.D. Whitman, *The Aircraft Reactor Experiment- Operation*. Nuclear Science and Engineering, 1957. **2**(6): p. 841-853.
29. W.K. Ergen, E.S Bettis, R.W. Schroeder, G.A Cristy, H.W Savage, R.G Affel, and I.F. Hemphill, *The Aircraft Reactor Experiment-Design and Construction*. Nuclear Science and Engineering, 1957. **2**(6): p. 804-825.
30. C.C. James, *Security Policy at the Dawn of the Nuclear Age: The Case of the Aircraft Nuclear Propulsion Project in Handbook of Global International Policy* S.S. Nagel, Editor. 2000, Marcel Dekker. p. 428-429.
31. D.F. Williams, L.M. Toth, and K.T. Clarno, *Assessment of Candidate Molten Salt Coolants for the Advanced High-Temperature Reactor (AHTR)*. 2006, Nuclear Science and Technology Division ORNL.
32. C.W. Forsberg, *Hydrogen, nuclear energy, and the advanced high-temperature reactor*. International Journal of Hydrogen Energy, 2003. **28**(10): p. 1073-1081.
33. R.C. Briant and A.M. Weinberg, *Molten fluorides as power reactor fuels*. Nuclear Science and Engineering, 1957. **2**(6): p. 797-803.
34. D.F. Williams and L.M. Toth, *Chemical considerations for the selection of the coolant for the advanced high-temperature reactor*. . 2005, Oak Ridge National Laboratory: Oak Ridge, Tennessee.
35. W.R. Grimes, *Molten Salt Reactor Chemistry*. Nuclear Applications and Technology, 1969. **8**: p. 137-155.
36. K. Sridharan and T.R. Allen, *Corrosion in Molten Salts* in *Molten Salts Chemistry*, H. Groult and F. Lantelme, Editors. 2013, Elsevier: Oxford. p. 241-267.
37. C.E. Housecroft and A.G. Sharpe, *Inorganic Chemistry*. 2005, Essex: Pearson Education Limited.
38. E.L. Compere, H.C. Savage, and J.M. Baker, *High intensity gamma irradiation of molten sodium fluoroborate-sodium fluoride eutectic salt*. Journal of Nuclear Materials, 1970. **34**(1): p. 97-100.
39. R.B. Briggs, *Molten Salt Reactor Program Semiannual Progress Report*. 1964, ORNL.
40. B.M. Elsheikh, *Safety assessment of molten salt reactors in comparison with light water reactors*. Journal of Radiation Research and Applied Sciences, 2013. **6**(2): p. 63-70.
41. D.F. Williams and K.T. Clarno, *Evaluation of Salt Coolants for Reactor Applications*. Nuclear Technology, 2008. **163**: p. 330-343.
42. V. Ignatiev and A. Surenkov, *Material Performance in Molten Salts*. Vol. 5. 2012. 221-250.
43. S. Delpéch, C. Cabet, C. Slim, and G.S. Picard, *Molten fluorides for nuclear applications*. Materials Today, 2010. **13**(12): p. 34-41.
44. R. Serrano-López, J. Fradera, and S. Cuesta-López, *Molten salts database for energy applications*. Chemical Engineering and Processing: Process Intensification, 2013. **73**: p. 87-102.
45. C.N.A.C.Z. Bahri, W.a.M. Al-Areqi, M.I.F.M. Ruf, and A.A. Majid, *Characteristic of molten fluoride salt system LiF-BeF<sub>2</sub> (Flibe) and LiF-NaF-KF (Flinak) as coolant and fuel carrier in molten salt reactor (MSR)*. AIP Conference Proceedings, 2017. **1799**(1): p. 040008.
46. L.S. Richardson, D.C. Vreeland, and W.D. Manly, *Corrosion of Molten Fluorides*. Oak Ridge National Laboratory, 1952. **ORNL-1491**.
47. M. Sarvghad, T.A. Steinberg, and G. Will, *Corrosion of stainless steel 316 in eutectic molten salts for thermal energy storage*. Solar Energy, 2018. **172**: p. 198-203.

48. W.-J. Cheng, D.-J. Chen, and C.-J. Wang, *High-temperature corrosion of Cr–Mo steel in molten LiNO<sub>3</sub>–NaNO<sub>3</sub>–KNO<sub>3</sub> eutectic salt for thermal energy storage*. Solar Energy Materials and Solar Cells, 2015. **132**: p. 563-569.
49. H. Lee, G.-I. Park, K.-H. Kang, J.-M. Hur, J.-G. Kim, D.-H. Ahn, Y.-Z. Cho, and E.H. Kim, *Pyroprocessing technology development at KAERI*. Nuclear Engineering and Technology, 2011. **43**(4): p. 318-328.
50. L.C. Olson, *Materials Corrosion in Molten LiF–NaF–KF Eutectic Salt*, in *Department of Engineering Physics*. 2009, University of Wisconsin-Madison.
51. S. Fabre, C. Cabet, L. Cassayre, P. Chamelot, S. Delepech, J. Finne, L. Massot, and D. Noel, *Use of electrochemical techniques to study the corrosion of metals in model fluoride melts*. Journal of Nuclear Materials, 2013. **441**(1–3): p. 583-591.
52. L. Olson, K. Sridharan, M. Anderson, and T. Allen, *Intergranular corrosion of high temperature alloys in molten fluoride salts*. Materials at High Temperatures, 2010. **27**(2): p. 145-149.
53. H.E. McCoy, *Status of Materials Development for Molten Salt Reactors*. 1978, Oak Ridge National Laboratory
54. D.T. Llewellyn and R.C. Hudd, *Steels: Metallurgy and Applications*. 1998: Butterworth Heinemann.
55. W.D. Manly, J. G. M. Adamson, J.H. Coobs, J.H. DeVan, D.A. Douglas, E.E. Hoffman, and P. Patriarca, *Aircraft Reactor Experiment- Metallurgical Aspects*. 1957, Oak Ridge National Laboratory.
56. A. Nishikata, H. Numata, and T. Tsuru, *Electrochemistry of molten salt corrosion*. Materials Science and Engineering: A, 1991. **146**(1): p. 15-31.
57. E.W. Collings and H.W. King. *The Metal Science of Stainless Steel in 107th AIME Annual Meeting*. 1978. Denver, Colorado: The Metallurgy Society of AIME.
58. U. Kamachi Mudali and B. Raj, *Corrosion science and technology: mechanism, mitigation and monitoring*. 2008, India: Narosa Publishing House.
59. Joseph R. Davis, *Corrosion: Understanding the Basics*. 2000: ASM International.
60. J.R. Davis, *Stainless Steels*. ASM Specialty Handbook (R) 1999: ASM International.
61. M.G. Fontana and N.D. Greene, *Corrosion Engineering*. 1978: McGraw-Hill.
62. Z. Ahmad, *CHAPTER 2 - BASIC CONCEPTS IN CORROSION*, in *Principles of Corrosion Engineering and Corrosion Control*, Z. Ahmad, Editor. 2006, Butterworth-Heinemann: Oxford. p. 9-56.
63. Naval Civil Engineering Laboratory, *Forms of Corrosion I: Uniform Corrosion/no Attack*. 1985: Department of the Navy, Naval Civil Engineering Laboratory.
64. A.J. Sedriks and O.S. Zaroog, *Corrosion of Stainless Steels*, in *Reference Module in Materials Science and Materials Engineering*. 2017, Elsevier.
65. E. McCafferty, *Introduction to Corrosion Science*. 2010: Springer New York.
66. L.C. Olson, J.W. Ambrosek, K. Sridharan, M.H. Anderson, and T.R. Allen, *Materials corrosion in molten LiF–NaF–KF salt*. Journal of Fluorine Chemistry, 2009. **130**(1): p. 67-73.
67. M.F. McGuire, *Stainless Steels for Design Engineers*, ed. A. International. Vol. Chapter 6. 2008.
68. C.E. Sessions and T.S. Lundy, *Diffusion of titanium in modified hastelloy N*. Journal of Nuclear Materials, 1969. **31**(3): p. 316-322.
69. J.H. DeVan, *Effect of Alloying Additions on Corrosion Behavior of Nickel-Molybdenum Alloys in Fused Fluoride Mixtures (thesis)*. 1969, Oak Ridge National Laboratory
70. J.H. DeVan and R.B. Evans, *Corrosion Behavior of Reactor Materials in Fluoride Salt Mixtures*. 1962, Oak Ridge National Laboratory.
71. F.-Y. Ouyang, C.-H. Chang, B.-C. You, T.-K. Yeh, and J.-J. Kai, *Effect of moisture on corrosion of Ni-based alloys in molten alkali fluoride FLiNaK salt environments*. Journal of Nuclear Materials, 2013. **437**(1–3): p. 201-207.

72. J.W. Koger, *Corrosion and Mass Transfer Characteristics of NaBF<sub>4</sub>-NaF (92-8 mol%) in Hastelloy N*. 1972, Oak Ridge National Laboratory.
73. J.W. Koger, *Effect of FeF<sub>2</sub> addition on mass transfer in a Hastelloy N- LiF-BeF<sub>2</sub>-UF<sub>4</sub> thermal convection loop*. 1972, Oak Ridge National Laboratory.
74. W. Ren, D. F. Wilson, G. Muralidharan, and D.E. Holcomb. *Considerations of Alloy N for Fluoride Salt Cooled High Temperature Reactor Applications*. in *Proceedings of the ASME 2011 Pressure Vessels & Piping Division Conference 2011*. Baltimore, Maryland, USA.
75. D.E. Holcomb, G.F. Flanagan, B.W. Patton, J.C. Gehin, R.L. Howard, and T.J. Harrison, *Fast Spectrum Molten Salt Reactor Options*. 2011, Oak Ridge National Laboratory.
76. Y. Hosoya, T. Terai, T. Yoneoka, and S. Tanaka, *Compatibility of structural materials with molten chloride mixture at high temperature*. *Journal of Nuclear Materials*, 1997. **248**: p. 348-353.
77. J.W. Ambrosek, *Molten Chloride Salts for Heat Transfer in Nuclear Systems*, in *Engineering Physics*. 2011, The University of Wisconsin - Madison.
78. I.N. Ozeryanaya, *Corrosion of metals by molten salts in heat-treatment processes*. *Metal Science and Heat Treatment*, 1985. **27**(3): p. 184-188.
79. V. Ignatiev and A. Surenkov, *Alloys compatibility in molten salt fluorides: Kurchatov Institute related experience*. *Journal of Nuclear Materials*, 2013. **441**(1-3): p. 592-603.
80. K. Vignarooban, P. Pugazhendhi, C. Tucker, D. Gervasio, and A.M. Kannan, *Corrosion resistance of Hastelloys in molten metal chloride heat transfer fluids for concentrating solar power applications*. *Solar Energy*, 2014. **103**: p. 62.
81. S.-H. Cho, J.-M. Hur, C.-S. Seo, and S.-W. Park, *High temperature corrosion of superalloys in a molten salt under an oxidizing atmosphere*. *Journal of Alloys and Compounds*, 2008. **452**(1): p. 11-15.
82. J.R. Reiser, J.H. DeVan, and E.J. Lawrence, *Compatibility of molten salts with type 316 stainless steel and lithium*. *Journal of Nuclear Materials*, 1979. **85**: p. 295-298.
83. P.F. Tortorelli, J.H. DeVan, and J.R. Keiser, *Corrosion of type 316 stainless steel in molten LiF-LiCl-LiBr*. *Journal of Nuclear Materials*, 1981. **103**: p. 675-680.
84. Sigma Aldrich, *Sodium Chloride Datasheet*. 2014.
85. Y. Shinata, F. Takahashi, and K. Hashiura, *Proceedings of the First International Symposium on High Temperature Corrosion of Materials and Coatings for Energy Systems and Turboengines NaCl-induced hot corrosion of stainless steels*. *Materials Science and Engineering*, 1987. **87**: p. 399-405.
86. N. Hiramatsu, Y. Uematsu, T. Tanaka, and M. Kinugasa, *Effects of alloying elements on NaCl-induced hot corrosion of stainless steels*. *Proceedings of the 2nd International symposium on High Temperature Corrosion of Advanced Materials and Coatings*, *Materials Science and Engineering: A*, 1989. **120**: p. 319-328.
87. I. Polovov, A. Abramov, O. I. Rebrin, V. Volkovich, E. Denisov, T. Griffiths, I. May, and H. Kinoshita, *Corrosion of Stainless Steels in NaCl-KCl Based Melts*. Vol. 33. 2010. 321-327.
88. A.R. Shankar and U.K. Mudali, *Corrosion of type 316L stainless steel in molten LiCl-KCl salt*. *Materials and Corrosion*, 2008. **59**(11): p. 878-882.
89. R.S. Sellers, M.H. Anderson, K. Sridharan, and T.R. Allen, *Failure analysis of 316L stainless steel crucible by molten fluoride salt interaction with clay bonded silicon carbide*. *Engineering Failure Analysis*, 2014. **42**: p. 38-44.
90. A. Kruiženga and D. Gill, *Corrosion of iron stainless steels in molten nitrate salt*. *Energy Procedia*, 2014. **49**: p. 878-887.
91. J. Olsson and B. Wallen, *Experience with a high molybdenum stainless steel in saline environments*. *Desalination*, 1983. **44**(1): p. 241-254.
92. B. Wällén, M. Liljas, and P. Stenvall, *A new high-molybdenum, high-nitrogen stainless steel*. *Materials & Design*, 1992. **13**(6): p. 329-333.

93. A.U. Malik, N.A. Siddiqi, and I.N. Andijani, *Corrosion behavior of some highly alloyed stainless steels in seawater*. *Desalination*, 1994. **97**(1): p. 189-197.
94. R. Muro, M. Neighbor, L. Shoemaker, and J. Crum, *An Advanced Super-Austenitic Stainless Steel Offers Economical And Technical Advantages Over Nickel-Base Corrosion-Resistant Alloys In The Process Industries*. 2010, NACE International.